Journal of Crystal Growth 439 (2016) 99–103

Contents lists available at ScienceDirect

Journal of Crystal Growth

journal homepage: www.elsevier.com/locate/jcrysgro

Towards defect-free epitaxial CdTe and MgCdTe layers grown on InSb (001) substrates

Jing Lu [a,b,*], Michael J. DiNezza [a,c], Xin-Hao Zhao [a,b], Shi Liu [a,c], Yong-Hang Zhang [a,c], Andras Kovacs [d], Rafal E. Dunin-Borkowski [d], David J. Smith [a,e]

[a] Center for Photonics Innovation, Arizona State University, Tempe, AZ 85287, USA
[b] School for Engineering of Matter, Transport and Energy, Arizona State University, Tempe, AZ 85287, USA
[c] School of Electrical, Computer and Energy Engineering, Arizona State University, Tempe, AZ 85287, USA
[d] Ernst Ruska-Centre for Microscopy and Spectroscopy with Electrons, Forschungszentrum Jülich, Jülich 52425, Germany
[e] Department of Physics, Arizona State University, Tempe, AZ 85287, USA

ARTICLE INFO

Article history:
Received 2 July 2015
Received in revised form
15 January 2016
Accepted 18 January 2016
Communicated by: E. Calleja
Available online 24 January 2016

Keywords:
A1. Defects
A1. Interfaces
A3. Molecular beam epitaxy
B1. Antimonides
B1. Tellurides
B2. Semiconducting II–VI

ABSTRACT

A series of three CdTe/$Mg_xCd_{1-x}Te$ ($x \sim 0.24$) double heterostructures grown by molecular beam epitaxy on InSb (001) substrates at temperatures in the range of 235–295 °C have been studied using conventional and advanced electron microscopy techniques. Defect analysis based on bright-field electron micrographs indicates that the structure grown at 265 °C has the best structural quality of the series, while structures grown at 30 °C lower or higher temperature show highly defective morphology. Geometric phase analysis of the CdTe/InSb interface for the sample grown at 265 °C reveals minimal interfacial elastic strain, and there is no visible evidence of interfacial defect formation in aberration-corrected electron micrographs of this particular sample. Such high quality CdTe epitaxial layers should provide the basis for applications such as photo-detectors and multi-junction solar cells.

1. Introduction

The interest in epitaxial thin films of CdTe (bandgap of 1.51 eV at room temperature) grown by molecular beam epitaxy (MBE) began in the early 1980s [1] because of potential applications in optoelectronic devices (e.g. infrared photo-detectors, solar cells) and as intermediary buffers for the growth of HgCdTe alloys on economic substrates [2]. The use of InSb as a candidate substrate for CdTe growth appears ideal because the two materials are nearly lattice-matched ($|\Delta a|/a \leq 5 \times 10^{-4}$ at room temperature), and they have highly similar thermal expansion coefficients. However, even with the application of Cd/Te flux ratios of greater than 1 during growth, defective interfacial III–VI structures still appear to be formed [3]. Interfacial compounds with different lattice parameters are liable to induce strain at the interface and possibly contribute to the formation of extended defects. Through proper handling of MBE growth parameters such as substrate surface preparation, growth temperature [4], and, most importantly, introduction of an intermediate InSb buffer layer in a dual-chamber MBE system [5], epitaxial CdTe films with high structural quality have recently been obtained [6]. One remaining complication for CdTe growth on InSb lies in the fact that CdTe (II–VI compound) and InSb (III–V compound) are heterovalent compound semiconductors. The possible formation of an interfacial III–VI alloy region due to inter-diffusion has been investigated by soft X-ray photoelectron spectroscopy (XPS) [7] and Raman spectroscopy [8]. However, there have so far been no published electron microscopy observations of any such interfacial compounds.

The characterization by X-ray diffraction (XRD) of epitaxial CdTe films grown on InSb substrates at different substrate temperatures has indicated that the full-width at half-maximum value of the CdTe XRD peak may not be a strong indication of the structural quality [9]. Thus, alternative techniques such as photoluminescence and cross-sectional transmission electron microscopy (XTEM) need to be combined to provide a more comprehensive characterization of the CdTe epilayer. In this study, conventional and aberration-corrected TEM imaging have been used to characterize the structural quality of epitaxial CdTe/$Mg_xCd_{1-x}Te$ ($x \sim 0.24$) double heterostructures grown on (001) InSb substrates with intermediate InSb and CdTe buffer layers. The strain distribution across the CdTe/InSb interface has also been investigated using the technique of geometric phase analysis [10].

* Corresponding author at: Physical Science Building B-344, Arizona State University, Tempe, AZ, 85287, USA. Tel.: +1-480-965-9815.
E-mail address: jinglu2@asu.edu (J. Lu).

http://dx.doi.org/10.1016/j.jcrysgro.2016.01.015
0022-0248/

2. Experimental details

The specimens under investigation were grown in a dual-chamber VG V80H MBE system with separate III–V and II–VI chambers connected by an ultrahigh-vacuum (UHV) transfer chamber. A schematic of the as-grown structures is shown in Fig. 1. First, InSb buffer layers of 500-nm thickness were grown on InSb (001) substrates in the III–V chamber. Monitoring *in situ* using reflection high-energy electron diffraction (RHEED) confirmed that the InSb surface oxide had been completely removed and that the InSb buffer layers had excellent crystallinity. The quality of the InSb buffer layers in all cases was later confirmed in the XTEM images. The wafers were then transferred to the II–VI chamber under UHV to receive Cd flux treatment prior to CdTe growth to suppress the possible extensive formation of interfacial III–VI compound. The Cd/Te flux ratio during growth was kept fixed at 1.5:1 after an initial two-minute period with a Cd/Te ratio of 3.5:1. RHEED was used throughout to monitor the II–VI growth [6]. As the CdTe growth was initiated, the RHEED pattern invariably turned hazy during a transition from the InSb to the CdTe pattern. At low substrate temperature (235 °C), the transition to clear 2×1 and $c(2\times2)$ patterns, which were used to confirm the Cd-rich condition, occurred quite rapidly compared with the growths done at higher temperature. After growth of the 500-nm-thick CdTe buffer layer, the CdTe/$Mg_xCd_{1-x}Te$ double heterostructure was grown, with the 1-μm-thick CdTe film sandwiched between two 30-nm-thick $Mg_xCd_{1-x}Te$ barrier layers with nominal Mg composition of 24%. The growth temperature was systematically varied (235 °C, 265 °C and 295 °C) while all other growth conditions were kept fixed.

Because of the known sensitivity of CdTe to argon-ion-milling [11,12], precautions need to be taken to ensure that the microstructure of CdTe epilayers observed via TEM is representative of the as-grown structure. Hence, argon-ion-milling should be performed using a liquid-nitrogen-cooled specimen holder [11,13]. Moreover, adequate thickness of the thinned film should be maintained prior to final milling to eliminate plastic deformation induced during post-growth mechanical polishing [14]. Most samples observed here were prepared for TEM observation along ⟨110⟩-type projections using traditional mechanical polishing and dimple grinding, followed by argon-ion-milling (maximum beam energy 2.2 keV) under liquid-nitrogen cooling in an effort to reduce ion-beam damage. One sample was prepared using low-voltage focused-ion-beam milling followed by ion-beam cleaning at 500 eV using a Fischione NanoMill. Electron microscopy was performed using a JEOL JEM-4000EX high resolution electron microscope with an accelerating voltage of 400 kV and structural resolution of 1.7 Å, and an aberration-corrected FEI-Titan 80–200 (scanning) transmission electron microscope (STEM) with sub-Å resolution remotely operated at 200 keV. Geometric phase analysis (GPA) was applied to the as-recorded aberration-corrected high-angle annular dark-field (HAADF) STEM images using a dedicated script in order to extract information about the strain distribution across the CdTe/InSb interfaces [15].

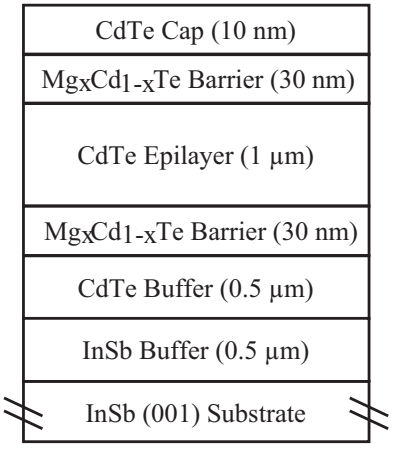

Fig. 1. Schematic (not to scale) showing the CdTe/$Mg_xCd_{1-x}Te$ double heterostructure, as grown on (001) InSb substrate, with intermediate InSb buffer, CdTe buffer and capping layers.

3. Results and discussion

Growth temperature had a major impact on the film morphology. As shown in the bright-field (BF) XTEM image in Fig. 2(a), many dislocations and threading defects were present in the lower part of the film grown at 235 °C, both in the CdTe buffer and also in the CdTe/$Mg_xCd_{1-x}Te$ double heterostructure regions. Most defects seemed to originate at or near the CdTe/InSb buffer interface, although there was no evidence for any Te precipitates, and the defect density dropped off considerably as the growth continued. Fig. 2(b) is a representative image showing the upper part of the heterostructure, and much less defects are visible in this region. Defect densities were estimated from the cross-sectional electron micrographs to range from $>10^9\,cm^{-2}$ near the CdTe/InSb interface to ~mid-$10^7\,cm^{-2}$ near the top surface. Ion-milling damage in CdTe has been identified previously as consisting primarily of planar-faulted dislocation loops with a density that is independent of sample thickness along the electron beam direction [11,16]. This is clearly not the situation here since the defect density steadily decreases moving away from the substrate.

Similar highly-defective film morphology was also observed for the structure grown at 295 °C as shown in Fig. 3. The bottom part of

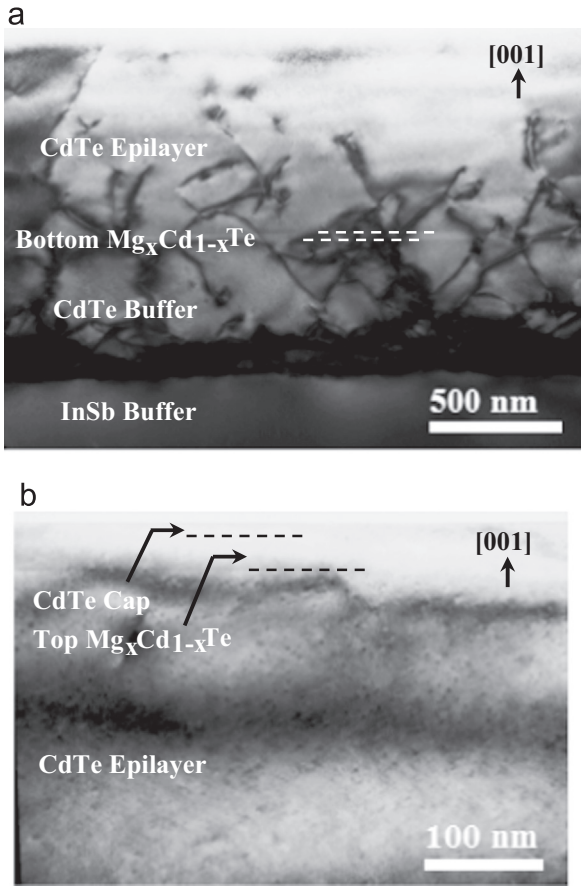

Fig. 2. BF XTEM images of the CdTe/$Mg_xCd_{1-x}Te$ double heterostructure grown at 235 °C: (a) lower region (close to the substrate); (b) upper region.

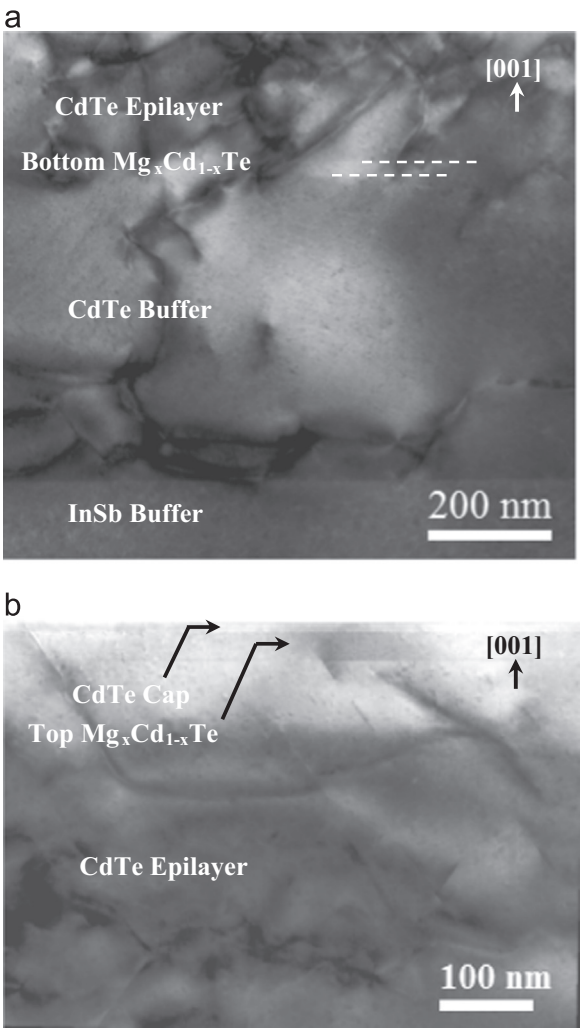

Fig. 3. BF XTEM images of the $CdTe/Mg_xCd_{1-x}Te$ double heterostructure grown at 295 °C: (a) lower region (close to the substrate); (b) upper region.

the double heterostructure for this sample had a very complicated network of entangled defects. The defect density decreased from $\sim 10^8$ cm^{-2} moving away from the CdTe/InSb interface but quite a few stacking fault (SF) defects and dislocations, perhaps $\sim 10^7$ cm^{-2}, were still observed in the upper region of the structure. The defective nature of the films grown at 235 °C and 295 °C is considered as unlikely to be due to sample preparation artifacts, because the sample grown at 265 °C, which showed very few defects, has been prepared for TEM observation using the same procedure.

The sample showing the best structural quality of this series was obtained from the growth at 265 °C. A representative BF XTEM image of the $CdTe/Mg_xCd_{1-x}Te$ double heterostructure grown at this temperature is shown in Fig. 4(a). Very few extended defects were visible, although SF defects were very occasionally seen, as shown by the example in Fig. 4(b). The lateral extent of this SF was not clear because only part of the fault structure was captured in this cross-sectional micrograph. The bottom $Mg_xCd_{1-x}Te$ barrier layer is clearly visible and free of defects, while the CdTe/InSb interface can also be identified due to slight differences in diffraction conditions. No extended defects were visible at this interface across several tens of microns of viewing area. Aberration-corrected HAADF and BF STEM images (Fig. 5) showed coherent defect-free interfaces between the CdTe and $Mg_xCd_{1-x}Te$ layer, and the top surface had excellent crystallinity. The minority carrier lifetime of this sample was measured using time-resolved photoluminescence (TRPL) to be 86 ns, which was

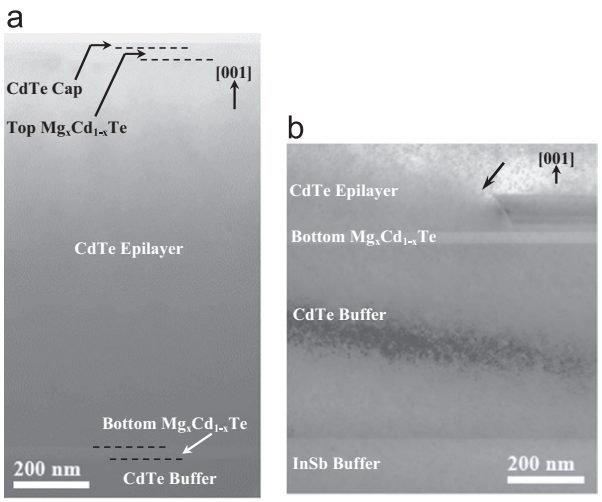

Fig. 4. (a) BF XTEM image showing the entire $CdTe/Mg_xCd_{1-x}Te$ double heterostructure grown at 265 °C, (b) bottom region, showing an isolated stacking fault defect (arrowed) in the lower part of the CdTe film.

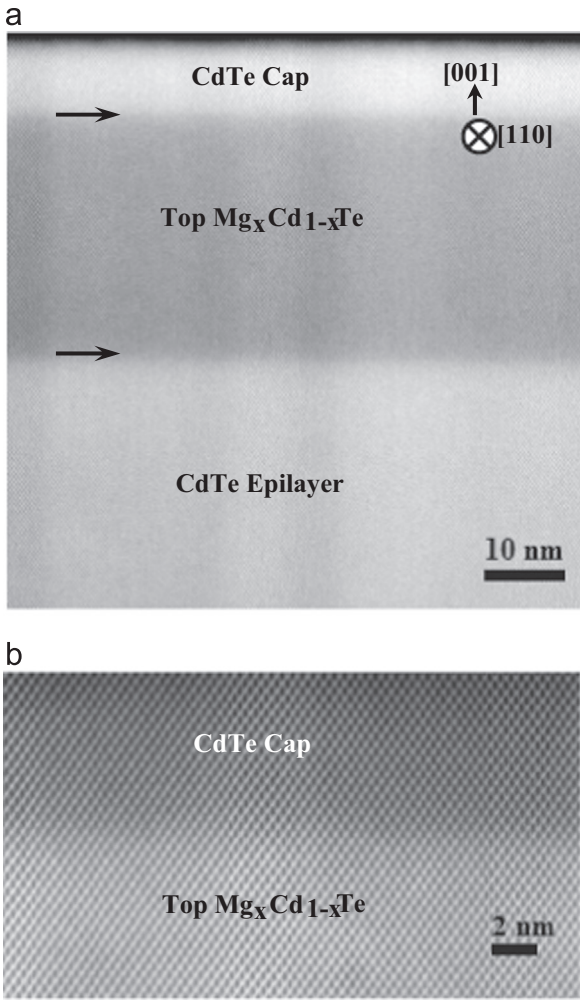

Fig. 5. (a) Aberration-corrected HAADF STEM image showing the upper region of the double heterostructure grown at 265 °C, with coherent, defect-free $CdTe/Mg_xCd_{1-x}Te$ interfaces (arrowed); (b) aberration-corrected BF STEM image of the top $CdTe/Mg_xCd_{1-x}Te$ interface (HAADF collection angle of 69–200 mrad; BF collection angle of 36.8 mrad).

the longest lifetime measured of this series of samples [17]. For comparison, the minority carrier lifetimes of the samples grown at 235 °C and 295 °C were 35 ns and 73 ns, respectively [17,18].

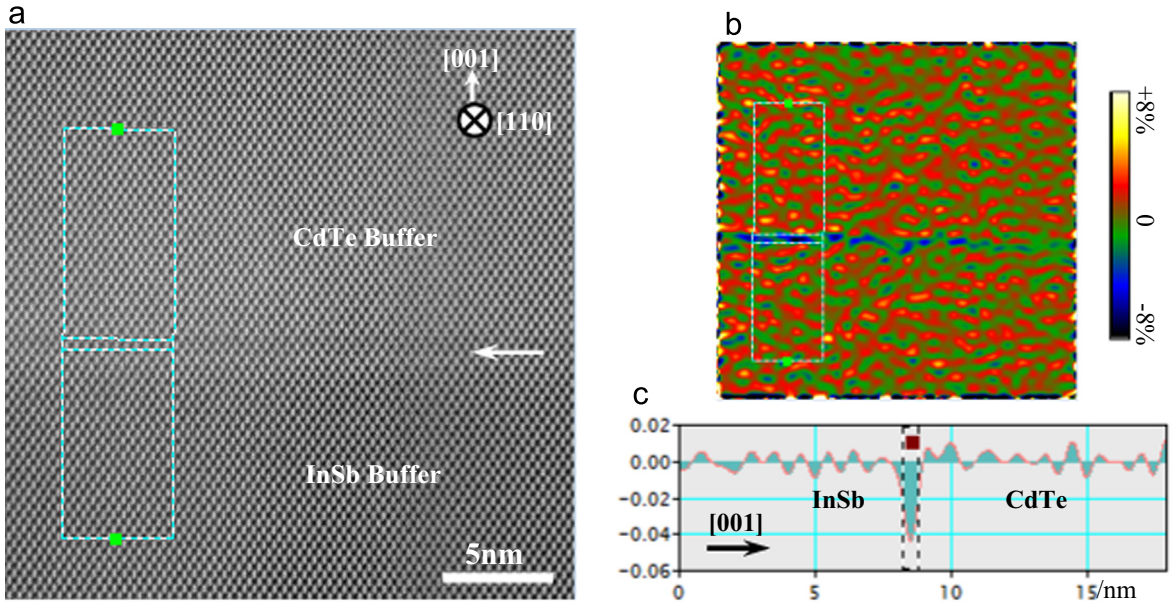

Fig. 6. (a) Aberration-corrected HAADF STEM image of sample grown at 265 °C showing the CdTe/InSb interface; (b) out-of-plane strain map obtained from GPA analysis; (c) line profile of out-of-plane strain extracted from the strain map averaged perpendicular to the growth direction (diffraction spots from two {111} planes were selected for GPA calculation).

The non-monotonic dependence of defect density and carrier lifetime on growth temperature can be reasonably understood. There are many examples of epitaxial heterostructures reported in the literature where there is a well-defined temperature range for optimal growth, with low temperatures being limited mostly by surface mobility, and higher temperatures being constrained by inter-diffusion. In our experiments, the Cd/Te flux ratio of 1.5:1 (3.5:1 for the initial 2 min) was maintained continuously to ensure a Cd-rich surface, and this condition was confirmed by the 2×1 and $c(2 \times 2)$ RHEED patterns observed at all growth temperatures. At the lower growth temperature, the mobility of atoms on the surface may well be low, and this effect is apparently manifested by the defective epilayer observed. In reference [4] Chew et al. reported the formation of polycrystalline CdTe and Te precipitates at very low growth temperature, < 150 °C, which is considerably lower than the temperature used here. We observed networks of extended defects, but no evidence for Te precipitates in the sample grown at 235 °C. At the higher growth temperature, inter-diffusion across the interface is likely to be enhanced, and could easily deteriorate the coherence of the CdTe epilayer in the vicinity of the interface. For regions away from the interface, the influence of such diffusion is reduced. This helps explain why the minority carrier lifetime measured in this sample was higher than that measured in the sample grown at the lowest temperature; the upper region of this epilayer, which is effectively where PL is probing, is relatively less defective for the highest temperature sample.

In addition, this particular batch of samples did not lend itself to providing accurate quantitative estimates of defect density as desired. There are several reasons, which can be explained as follows: (i) The entire II–VI heterostructure, as illustrated in Fig. 1, is more than 1500 nm in thickness and consists of several different thick and thin layers. Plan-view geometry, which is usually preferred for estimating defect densities, will not be able to differentiate between the different layers and interfaces, and the bottom CdTe/InSb interface is too deep and unlikely to be accessible; (ii) the cross-section geometry can obviously be used for highly defective materials and can provide a 'ball-park' qualitative guesstimate of defect density, as we have done in the text for the samples grown at low (235 °C) and high (295 °C) temperatures. However, for material of exceptionally high quality, such as the sample grown at 265 °C, TEM techniques are no longer viable and one would then be obliged to use a different approach to estimate defect density, such as XRD FWHM, electroluminescence, or chemical etchant EPD. However, these may not be feasible with the current complicated heterostructure. A more systematic study of 'simple' CdTe/InSb heterostructures for this purpose will be carried out in the not-too-distant future. Meanwhile, several tens of microns of the CdTe/InSb interface for the sample grown at 265 °C have been examined, and no evidence for the formation of even a single extended defect has been seen.

The CdTe/InSb interface has been a subject of considerable interest for microscopists ever since the early trials of CdTe growth on InSb [16]. X-ray photoemission spectroscopy and Raman spectroscopy were used previously to extract information about the interface, and the possible formation of an interfacial compound with a much smaller lattice constant (III–VI compound) was suggested. Thus, aberration-corrected HAADF STEM images were taken of the CdTe/InSb interface for the sample grown at 265 °C, to explore the strain distribution, i.e., in-plane strain, out-of-plane strain, rotation and shear, across the interfacial layers. The out-of-plane strain in the [001] growth direction is defined by the expression:

$$\xi_{zz} = \frac{c_{\text{alloy}} - c_{\text{reference}}}{c_{\text{reference}}} \quad (1)$$

where c is the lattice constant along the growth direction, and the InSb buffer region is used as the zero-strain reference for all strain analysis. Images with the interface oriented vertically and horizontally were recorded for analysis of the out-of-plane and in-plane strain, respectively, to eliminate the possible influence of scan distortion on the analysis.

The in-plane strain, i.e., strain within the (001) growth plane, and the rotation and shear strain, were negligible (below the detectability of GPA analysis here) across the interface and over the field of view (not shown here). Fig. 6(a) is a representative HAADF STEM image of the CdTe/InSb buffer interface recorded with the interface vertically oriented (rotated post-recording to have the growth direction pointing upwards), and is used to extract the out-of-plane strain map and line profile, as shown in Fig. 6(b) and (c), respectively. The CdTe was on-average under slight compressive strain, which is attributed to its slightly larger lattice parameter compared to the InSb buffer. A sharp tensile

spike was observed right at the CdTe/InSb interface (arrowed), while the strain in the adjacent InSb and CdTe regions is relatively uniform. The width of the spike is ~0.7 nm, while the GPA spatial resolution defined by this analysis is 0.7 nm. Such a sharp spike is an indication of a rigid-body displacement across a few monolayers at the interface (rather than elastic strain), but the analysis shows no evidence for the formation of any interfacial defects, although the possibility of an atomically thin layer of a II–V compound cannot be excluded. The slightly different thermal expansion/contraction behavior of CdTe and InSb did not cause noticeable lattice disruption.

4. Conclusions

Epitaxial CdTe/$Mg_xCd_{1-x}Te$ ($x \sim 0.24$) double heterostructures grown at different temperatures on InSb (100) substrates were studied by various transmission electron microscopy techniques. The optimum growth window was quite narrow. The CdTe epilayers grown at 265 °C had exceptional structural quality and the CdTe/InSb interface showed no visible extended defects, whereas growth temperatures of 30 °C higher or lower gave highly defective films. Geometric phase analysis of aberration-corrected HAADF STEM images indicated that the CdTe/InSb interface was under minimal elastic strain but with a minute rigid-body displacement, which was consistent with the absence of any structural features attributable to the presence of extensive interfacial compounds other than an atomically thin, possibly II–V, layer which is under further investigation. We are using HAADF as well as large collection-angle BF STEM imaging, in combination with spectroscopic techniques, to define the atomistic nature of the CdTe/InSb interface, and we expect to report the results of this investigation in the near future.

Acknowledgments

The authors gratefully acknowledge support from AFOSR (Grant no. FA9550-12-1-0444), Science Foundation Arizona (Grant no. SRG 0339-08) and the use of facilities in the John M. Cowley Center for High Resolution Electron Microscopy at Arizona State University.

References

[1] R.F.C. Farrow, G.R. Jones, G.M. Williams, I.M. Young, Appl. Phys. Lett. 39 (1981) 954–956.
[2] R.F.C. Farrow, J. Vac. Sci. Technol. A 3 (1985) 60–66.
[3] G.M. Williams, C.R. Whitehouse, A.G. Cullis, N.G. Chew, G.W. Blackmore, Appl. Phys. Lett. 53 (1988) 1847–1850.
[4] N.G. Chew, G.M. Williams, A.G. Cullis, Inst. Phys. Conf. 68 (1983) 437–440.
[5] R.F.C. Farrow, A.J. Noreika, F.A. Shirland, W.J. Takei, S. Wood, J. Greggi Jr., M. H. Francombe, J. Vac. Sci. Technol. A 2 (1984) 527–528.
[6] M.J. DiNezza, X.-H. Zhao, S. Liu, A.P. Kirk, Y.-H. Zhang, Appl. Phys. Lett. 103 (2013) 193901–193904.
[7] K.J. Mackey, P.M.G. Allen, W.G. Herrenden-Harker, R.H. Williams, Appl. Phys. Lett. 49 (1986) 354–358.
[8] D.R.T. Zahn, K.J. Mackey, R.H. Williams, Appl. Phys. Lett. 50 (1987) 742–746.
[9] Z.C. Feng, A. Mascarenhas, W.J. Choyke, R.F.C. Farrow, F.A. Shirland, W.J. Takei, Appl. Phys. Lett. 47 (1985) 24–26.
[10] M.J. Hytch, E. Snoeck, R. Kilaas, Ultramicroscopy 74 (1998) 131–146.
[11] A.G. Cullis, N.G. Chew, J.L. Hutchison, Ultramicroscopy 17 (1985) 203–211.
[12] T. Aoki, Y. Chang, G. Badano, J. Zhao, C. Grein, S. Sivananthan, D.J. Smith, J. Cryst. Growth 265 (2004) 224–234.
[13] C. Wang, S. Tobin, T. Parodos, J. Zhao, Y. Chang, S. Sivananthan, D.J. Smith, J. Vac. Sci. Technol. A 24 (2006) 995–1000.
[14] S. Wood, J. Greggi Jr., R.F.C. Farrow, W.J. Takei, F.A. Shirland, A.J. Noreika, J. Appl. Phys. 55 (1984) 4225–4231.
[15] Digital Micrograph script developed by C. Koch (Ulm).
[16] J.L. Hutchison, W.G. Waddington, A.G. Cullis, N.G. Chew, J. Microsc. 142 (1986) 153–162.
[17] X.-H. Zhao, M.J. DiNezza, S. Liu, S. Lin, Y. Zhao, Y.-H. Zhang, J. Vac. Sci. Technol. B 32 (040601) (2014) 1–4.
[18] X.-H. Zhao, M.J. DiNezza, S. Liu, Y. Zhao, Y.-H. Zhang, unpublished results.